Inorg. Chem. **2004**, *43*, 2330–2339

Poly[(2,2′-bipyridine)tetrakis(imidazolato)diiron(II)]: Structural and Spin-State Phase Transitions and Low-Temperature Magnetic Ordering in a Unique 2-Dimensional Material

Brian O. Patrick,[†] William M. Reiff,*[,‡] Victor Sánchez,[§] Alan Storr,*[,†] and Robert C. Thompson*[,†]

Department of Chemistry, University of British Columbia, Vancouver, BC, Canada V6T 1Z1, Department of Chemistry, Northeastern University, Boston, Massachusetts 02115, and Facultad de Quimica, Universidad Autonoma del Estado de Mexico, Toluca, Mexico CP 50120

Received May 23, 2003

Poly[(2,2′-bipyridine)tetrakis(imidazolato)diiron(II)] was synthesized by the reaction of ferrocene with imidazole in an excess of 2,2′- bipyridine in a Carius tube at 130 °C. Dc magnetic susceptibility studies at an applied field of 1000 G reveal that on cooling from room temperature, the material undergoes two structural phase transitions designated $\alpha \rightarrow \beta$ and $\beta \rightarrow \gamma$ at 151 and 133 K, respectively. On warming, the $\gamma \rightarrow \beta$ and $\beta \rightarrow \alpha$ transitions are observed at 137 and 151 K, respectively; a 4 K thermal hysteresis clearly detectable in the lower temperature $\beta \leftrightarrow \gamma$ transition. These structural phase transitions have also been studied by detailed, variable-temperature, ac susceptibility and Mössbauer spectroscopy techniques. Single-crystal X-ray diffraction studies done at 294, 143, and 113 K reveal 2, 12, and 6 unique iron centers in the α-, β-, and γ-forms, respectively. All three forms have the same basic structure involving 2D extended double layer sheets (bilayers) of alternating tetrahedral and octahedral irons singly bridged by imidazolate ligands, with the octahedral centers additionally coordinated by 2,2′-bipyridine ligands that occupy positions between the sheets. Magnetic susceptibility and bond length data reveal that in the γ-phase one in three six-coordinate sites corresponds to spin singlet ground-state iron(II); i.e., the overall $\alpha \rightarrow \gamma$ process involves a spin-crossover transition such that at least 1/6 of the iron sites in the γ-phase correspond to $S = 0$. This is supported by the low-temperature Mössbauer spectra of the γ-phase, which reveal the simultaneous presence of both $S = 2$ and $S = 0$ iron(II) centers. The compound magnetically orders, with a resultant small remnant magnetization, at low temperatures. The magnetic phase transition, studied by a combination of dc and ac susceptibility and Mössbauer techniques, occurs at $T_c \sim 6.5$ K.

Introduction

In recent years there has been considerable interest in molecular materials that undergo long-range ferromagnetic ordering below some critical temperature, so-called molecule-based magnets.[1−3] Materials in this class include complex metal cyanides,[4] organometallic systems,[5] and purely organic compounds.[6] Our own focus in this area has been on coordination polymers of paramagnetic first-row transition metals, especially iron(II) and cobalt(II) compounds incorporating bridging 1,3-diazolate ligands.[7] Materials of this type which we have characterized and which exhibit low-temperature magnetic ordering include three which have extended 3D lattice structures, $Fe_3(imid)_6(Himid)_2$,[7a] Fe(4-abimid)$_2$,[7b] and Fe(2-meimid)$_2$·0.13Cp_2Fe[7c] (where imid = imidazolate, 4-abimid = 4-azabenzimidazolate, 2-meimid =

* To whom correspondence should be addressed. E-mail: w.reiff@neu.edu (W.M.R.); storr@chem.ubc.ca (A.S.); thompson@chem.ubc.ca (R.C.T.). Telephone/fax: (617) 373-2381/(617) 373-8795 (W.M.R.); (604) 822-3962/(604) 822-2847 (A.S.); (604) 822-4979/(604) 822-2847 (R.C.T.).
† University of British Columbia.
‡ Northeastern University.
§ Universidad Autonoma del Estado de Mexico.

(1) Proceedings of the Conference on Molecule-based Magnets. Miller, J. S., Epstein, A. J., Eds. *Mol. Cryst. Liq. Cryst.* **1995**, 271−274. Proceedings of the Fifth International Conference on Molecule-based Magnets. Itoh, K., Miller, J. S., Takui, K., Eds. *Mol. Cryst. Liq. Cryst.* **1997**, 305−306.
(2) Gateschi, D. *Adv. Mater.* **1994**, *6*, 635.
(3) Kahn, O. *Acc. Chem. Res.* **2000**, *33*, 647.
(4) Ferlay, S.; Mallah, T.; Ouahes, R.; Veillet, P.; Verdaguer, M. *Nature* **1995**, *378*, 701.
(5) Miller, J. S. *Inorg. Chem.* **2000**, *39*, 4392.
(6) Banister, A. J.; Bricklebank, N.; Lavender, I.; Rawson, J. M.; Gregory, C. I.; Tanner, B. K.; Clegg, W.; Elsegood, M. R. J.; Palacio, F. *Angew. Chem., Int. Ed. Engl.* **1996**, *35*, 2533.

10.1021/ic030170n CCC: $27.50
Published on Web 03/10/2004

2-methylimidazolate, and Cp = cyclopentadienyl), and one, Fe(1-Me-2-S-imid)$_2$·0.5Cp$_2$Fe (where 1-Me-2-S-imid = 1-methyl 2- thioimidazolate), which has a 1D extended chain structure.[7d,e]

Recently, we reported preliminary studies on Fe$_2$(imid)$_4$(bipy) (where bipy = 2,2′-bipyridine), a new molecule-based magnet which has a novel double-layer 2D extended lattice structure at room temperature.[8] In the course of magnetically characterizing this material employing dc magnetization studies in an applied field of 10 000 G,[8] we discovered a clear discontinuity in the μ_{eff} versus T plot near 135 K. This observation coupled with preliminary evidence from X-ray diffraction studies that significant changes in cell parameters occur around this temperature prompted detailed and extensive variable-temperature studies of this compound employing the techniques of single-crystal X-ray diffraction, dc and ac susceptibilities, and Mössbauer spectroscopy. These studies, reported herein, reveal that the title compound, on cooling from 300 to 2 K, exhibits the novel property of undergoing structural phase transitions at around 151 and 135 K. Mössbauer studies suggest a $S = 0$ ground state at some of the six coordinate sites in the low-temperature phase. Additionally, there is a transition to a magnetically ordered state below 11 K.

Experimental Section

Synthesis. The synthesis of Fe$_2$(imid)$_4$(bipy) by the reaction of ferrocene with imidazole in an excess of 2,2′-bipyridine in a Carius tube at 130 °C was described previously.[8] Since the compound is air sensitive, all measurements were carried out in a dry nitrogen, helium, or argon environment.

Physical Measurements. Dc Magnetic susceptibility measurements were made on macroscopic crystals ground to a fine powder, utilizing a Quantum Design (MPMS) SQUID magnetometer. The sample holder and details regarding the use of the equipment have been described elsewhere.[9] Magnetic susceptibilities were corrected for the background signal of the sample holder and for diamagnetic susceptibilities of all atoms (-130×10^{-6} cm^3 mol^{-1}). Dc susceptibilities were measured from 2 to 300 K at 1000 G. The overall temperature change rate employed was ~0.2° min^{-1} in both cooling and heating modes. Field-cooled, zero-field-cooled, and remnant dc magnetization measurements were made from 2 to 12 K by employing an applied field of 50 G.

All ac magnetic susceptibilities were made using a Lake Shore Cryotronics Co. model 7000 ac susceptometer. Ac measurements on powdered samples were made over the temperature range 4.2−30 K in an ac field of 1 G at a frequency of 125 Hz and from 110 to 160 K in an ac field of 2.5 G at a frequency of 500 Hz.

The Mössbauer spectra were determined using a conventional constant-acceleration spectrometer operated in multichannel scaling mode. The γ-ray source (Du Pont-Merck Co.) consisted of 51.5 mCi of Co^{57} in a rhodium metal matrix that was maintained at ambient temperature. The spectrometer was calibrated using a 6 μm thick natural abundance iron foil. Isomer shifts are reported relative to the center of the magnetic hyperfine pattern of the latter foil (at ambient temperature) taken as zero velocity. The line widths of the innermost pair of $\Delta M_I = \pm 1$ transitions of the latter Zeeman pattern were reproducibly determined to be 0.214 mm/s. Sample temperature variation was achieved using a standard exchange gas liquid-helium cryostat (Cryo Industries of America, Inc.) with temperature measurement and control based on silicon diode thermometry in conjunction with a 10 μA excitation source (Lakeshore Cryotronics, Inc). Spectra were fit to unconstrained Lorentzians using the program ORIGIN (Microcal Software, Inc.).

The thermometry of the Mössbauer spectroscopy and ac susceptibility instrumentation (Si and GaAlAs diodes, respectively) used at Northeastern University was carefully cross-calibrated via detailed study of the magnetic ordering of a polycrystalline sample of pure anhydrous ferrous fluoride (Strem Chemical, 99.9%) whose purity was further verified via Mössbauer spectroscopy. FeF_2 has been shown by previous zero-field techniques (heat capacity[10] and Mössbauer spectroscopy[11]) as well as classical susceptibility study[12] to order antiferromagnetically at $T_N = 78.20 \pm 0.20$ K, a convenient temperature in the context of this study. Our values for T_N for FeF_2 via Mössbauer spectroscopy and ac susceptometry are within 0.5 K of the latter.

Table 1. Crystallographic Data

	α-phase	β-phase[a]	γ-phase
empirical formula	$C_{22}H_{20}Fe_2N_{10}$	$C_{22}H_{20}Fe_2N_{10}$	$C_{22}H_{20}Fe_2N_{10}$
fw	536.16	536.16	536.16
space group	$P\bar{1}$ (No. 2)	$P\bar{1}$ (No. 2)	$P\bar{1}$ (No. 2)
a, Å	10.507(4)	17.133(3)	10.4138(5)
b, Å	13.730(4)	18.530(1)	13.5075(5)
c, Å	9.188(3)	23.625(2)	26.060(1)
α, deg	106.51(3)	80.463(2)	104.530(2)
β, deg	108.32(3)	75.336(2)	93.892(2)
γ, deg	80.84(3)	80.839(3)	100.512(2)
V, Å^3	1202.9(7)	7101.2(2)	3464.0(2)
Z	2	12	6
ρ_{calc}, g/cm^3	1.480	1.505	1.542
T, K	294	143	113
λ, Å	0.710 69	0.710 69	0.710 69
μ, cm^{-1}	12.36	12.58	12.88
R1[b]	0.037	0.116	0.039
wR2[c]	0.093	0.279	0.110

[a] Refined isotropically. [b] $I > 2\sigma(I)$), $R1 = \sum||F_o| - |F_c||/\sum|F_o|$. [c] $wR2 = (\sum w(F_o^2 - F_c^2)^2/\sum wF_o^4)^{1/2}$ on all data.

X-ray Crystallographic Analysis. Crystallographic data for all three forms of Fe$_2$(imid)$_4$(bipy) are shown in Table 1. A green prism crystal of α-Fe$_2$(imid)$_4$(bipy) having approximate dimensions of 0.35 × 0.15 × 0.15 mm was mounted on a diffractometer (Rigaku AFC6S) and used for data collection at 294 K. Another crystal of α-Fe$_2$(imid)$_4$(bipy) having approximate dimensions of 0.45 × 0.35 × 0.20 mm was mounted on a diffractometer (Rigaku/ADSC CCD) and used for data collection at 113 K. It was important to establish that the polymorph at this temperature (γ-phase) is, in fact, a different temperature phase of the material and that we had not simply picked a different polymorph from the room temperature sample. To do this, the unit cell of the crystal used for the study at 113 K was determined initially at 173 K. The unit cell parameters were found to be the same as those obtained at 294 K, confirming

(7) (a) Rettig, S. J.; Storr, A.; Summers, D. A.; Thompson, R. C.; Trotter, J. *J. Am. Chem. Soc.* **1997**, *119*, 8675. (b) Rettig, S. J.; Sánchez, V.; Storr, A.; Thompson, R. C.; Trotter, J. *J. Chem. Soc., Dalton Trans.* **2000**, 3931. (c) Rettig, S. J.; Storr, A.; Summers, D. A.; Thompson, R. C.; Trotter, J. *Can. J. Chem.* **1999**, *77*, 425. (d) Rettig, S. J.; Sánchez, V.; Storr, A.; Thompson, R. C.; Trotter, J. *Inorg. Chem.* **1999**, *38*, 5920. (e) Reiff, W. M.; Sánchez, V.; Thompson, R. C.; Storr, A. *Polyhedron* **2001**, *20*, 1243.
(8) Patrick, B. O.; Reiff, W. M.; Sánchez, V.; Storr, A.; Thompson, R. C. *Polyhedron* **2001**, *20*, 1577.
(9) Ehlert, M. K.; Rettig, S. J.; Storr, A.; Thompson, R. C.; Trotter, J. *Can. J. Chem.* **1989**, *67*, 1970.
(10) Wertheim, G. K.; Buchanan, D. N. E. *Phys. Rev.* **1967**, *161*, 478.
(11) Stout, J. W.; Catalano, E. *Phys. Rev.* **1953**, *92*, 1575.
(12) Bizette, H. *Ann. Phys.* **1946**, *1* (12), 233.

Table 2. Selected Bond Lengths (Å) for α- and γ-$Fe_2(imid)_4(bipy)$ with Estimated Standard Deviations in Parentheses

		α-Phase[a]			
Fe(1)−N(1)	2.262(2)	Fe(1)−N(2)	2.299(3)	Fe(1)−N(3)	2.194(2)
Fe(1)−N(5)	2.153(2)	Fe(1)−N(8)[b]	2.190(2)	Fe(1)−N(10)[a]	2.153(2)
Fe(2)−N(4)[c]	2.022(2)	Fe(2)−N(6)	2.032(2)	Fe(2)−N(7)	2.027(2)
Fe(2)−N(9)	2.029(2)				
		γ-Phase[b]			
Fe1b−N2b	2.313(2)	Fe1a[d]−N8c	2.187(2)	Fe1b−N1b	2.217(3)
Fe2c−N9c	2.035(2)	Fe1b−N3b	2.207(2)	Fe2b−N4a	2.025(3)
Fe1b[e]−N10b	2.162(2)	Fe2c−N7c	2.040(2)	Fe1b[c]−N8b	2.194(2)
Fe2c[a]−N6c	2.037(3)	Fe1b−N5b	2.137(3)	Fe1c−N3c	2.011(2)
Fe1c−N5c	2.019(3)	Fe2b−N6b	2.018(3)	Fe2b−N9b	2.031(2)
Fe1c−N10a	2.016(2)	Fe2b−N7b	2.030(2)	Fe1c[b]−N8a	2.003(2)
Fe2c−N4c	2.025(3)	Fe1c−N1c	1.956(3)	Fe1a−N3a	2.186(2)
Fe1c−N2c	1.970(2)	Fe1a−N5a	2.152(3)	Fe2a−N4b	2.059(3)
Fe1a[a]−N10c	2.155(2)	Fe2a−N6a	2.055(3)	Fe1a−N1a	2.263(3)
Fe2a−N9a	2.034(2)	Fe1a−N2a	2.302(2)	Fe2a−N7a	2.038(2)

[a] Symmetry transformations used to generate equivalent atoms: (a) $-x + 2, -y, -z + 1$; (b) $-x + 1, -y, -z + 1$; (c) $-x + 2, -y, -z + 2$. [b] Symmetry transformations used to generate equivalent atoms: (a) $-x + 1, -y, -z + 1$; (b) $x - 1, y, z$; (c) $-x + 1, -y, -z$; (d) $-x, -y, -z + 1$; (e) $-x, -y, -z$; (f) $x + 1, y, z$.

the α-phase. The crystal was then cooled to 113 K at which temperature the cell parameters had changed to those of the γ-phase. A similar procedure was used in determining the structure of the β-phase. A crystal of α-$Fe_2(imid)_4(bipy)$ having approximate dimensions of 0.30 × 0.25 × 0.20 mm was mounted on a diffractometer (Rigaku/ADSC). When examined at 170 K, the crystal was found to have the same cell parameters as the α-phase. On cooling of this crystal to 143 K, the cell parameters had changed to those of the β-phase.

Final unit cell parameters were obtained by least-squares fitting on the setting angles for 7376 reflections (α), 18 019 reflections (β), and 21 062 reflections (γ) with $2\theta_{max} = 60.0°$ (α), 55.8° (β), and 56.1° (γ). The data were processed[13] and corrected for Lorentz and polarization effects. The structures were solved by direct methods[14] and expanded using Fourier techniques.[15]

While accurate structures were obtained for both the α- and γ-phases, the same cannot be said for the β-phase (see R1 and wR2 values in Table 1). The β-phase unit cell appears to be six times the size of the α-phase and twice the size of the γ-phase. The solution clearly shows disorder in the orientation of several of the imidazolate rings; however, subsequent anisotropic refinements appear to be unstable. The reason for this is unclear; however, the average intensity for each reflection in this structure ($\langle I/\sigma(I)\rangle = 4.7$) is significantly lower than for either the α- and γ-phases (9.7 and 9.1, respectively). This relatively weak data may result in the unsatisfactory refinement, or it may be indicative of some systematic problem with the data.

Selected bond lengths and bond angles for the α- and γ-phases are shown in Tables 2 and 3. Corresponding data for the β-phase are not included due to the unsatisfactory refinement of this phase. Final atomic coordinates and equivalent isotropic thermal parameters, hydrogen atom parameters, anisotropic thermal parameters, torsion angles, nonbonded contacts, and least-squares planes for the α- and γ-phases are included as Supporting Information.

Table 3. Selected Bond Angles (deg) for α- and γ-$[Fe_2(imid)_4(bipy)]_x$ with Estimated Standard Deviations in Parentheses

	α-Phase[a]		
N(1)−Fe(1)−N(2)	71.78(9)	N(1)−Fe(1)−N(3)	89.68(9)
N(1)−Fe(1)−N(5)	168.22(9)	N(1)−Fe(1)−N(8)[b]	88.91(8)
N(1)−Fe(1)−N(10)[a]	97.12(9)	N(2)−Fe(1)−N(3)	88.99(9)
N(2)−Fe(1)−N(5)	96.51(9)	N(2)−Fe(1)−N(8)[b]	83.61(9)
N(2)−Fe(1)−N(10)[a]	168.33(9)	N(3)−Fe(1)−N(5)	88.75(9)
N(3)−Fe(1)−N(8)[b]	172.53(9)	N(3)−Fe(1)−N(10)[a]	94.65(9)
N(5)−Fe(1)−N(8)[b]	91.14(9)	N(5)−Fe(1)−N(10)[a]	94.65(9)
N(8)−Fe(1)−N(10)[a]	92.80(9)	N(4)−Fe(2)−N(6)	111.3(1)
N(4)−Fe(2)−N(7)	110.15(9)	N(4)−Fe(2)−N(9)	106.96(9)
N(6)−Fe(2)−N(7)	105.33(9)	N(6)−Fe(2)−N(9)	105.47(9)
N(7)−Fe(2)−N(9)	117.6(1)		
	γ-Phase[b]		
N1b−Fe1b−N2b	72.50(9)	N2b−Fe1b−N3b	91.08(8)
N2b−Fe1b−N10b[e]	169.56(10)	N2b−Fe1b−N8b[c]	81.34(9)
N2b−Fe1b−N5b	96.72(9)	N1b−Fe1b−N3b	90.00(8)
N1b−Fe1b−N10b[e]	98.34(9)	N1b−Fe1b−N8b[c]	89.40(9)
N1b−Fe1b−N5b	169.18(9)	N3b−Fe1b−N10b[e]	93.96(9)
N3b−Fe1b−N8b[c]	172.21(9)	N3b−Fe1b−N5b	91.14(10)
N8b[d]−Fe1b−N10b[e]	93.81(9)	N5b−Fe1b−N10b[e]	92.32(10)
N5b−Fe1b−N8b[c]	88.01(10)	N6b−Fe2b−N9b	102.92(10)
N6b−Fe2b−N7b	108.71(10)	N4a−Fe2b−N6b	110.77(11)
N4a−Fe2b−N9b	107.34(9)	N4a−Fe2b−N7b	109.11(9)
N7b−Fe2b−N9b	117.81(10)	N3a−Fe1a−N5a	86.82(10)
N3a−Fe1a−N10c[a]	93.54(9)	N1a−Fe1a−N3a	87.42(9)
N2a−Fe1a−N3a	89.75(9)	N3a−Fe1a−N8c[d]	174.24(9)
N5a−Fe1a−N10c[a]	97.36(10)	N1a−Fe1a−N5a	163.38(9)
N2a−Fe1a−N5a	92.65(9)	N8c[d]−Fe1a−N10c[a]	92.21(9)
N1a−Fe1a−N10c	98.55(9)	N2a−Fe1a−N10c[a]	169.61(10)
N5a−Fe1a−N8c[d]	92.22(9)	N1a−Fe1a−N2a	71.73(9)
N1a−Fe1a−N8c[d]	91.95(9)	N2a−Fe1a−N8c[d]	84.61(8)
N4c−Fe2c−N9c	109.07(10)	N7c−Fe2c−N9c	114.73(10)
N6c[e]−Fe2c−N9c	104.21(10)	N4c−Fe2c−N7c	112.75(9)
N4c−Fe2c−N6c[a]	109.91(11)	N6c[a]−Fe2c−N7c	105.69(10)
N3c−Fe1c−N5c	88.40(10)	N3c−Fe1c−N10a	92.28(9)
N3c−Fe1c−N8a[f]	177.72(9)	N1c−Fe1c−N3c	90.88(10)
N2c−Fe1c−N3c	90.97(9)	N5c−Fe1c−N10a	89.18(10)
N5c−Fe1c−N8a[f]	91.73(10)	N1c−Fe1c−N5c	176.79(10)
N2c−Fe1c−N5c	95.13(10)	N8a[f]−Fe1c−N10a	90.00(9)
N1c−Fe1c−N10a	93.98(10)	N2c−Fe1c−N10a	174.68(11)
N1c−Fe1c−N8a[f]	88.86(10)	N2c−Fe1c−N8a	86.75(9)
N1c−Fe1c−N2c	81.76(10)	N4b−Fe2a−N6a	114.79(11)
N4b−Fe2a−N9a	105.94(10)	N4b−Fe2a−N7a	104.76(9)
N6a−Fe2a−N9a	102.70(10)	N6a−Fe2a−N7a	100.82(10)
N7a−Fe2a−N9a	128.26(10)		

[a] Symmetry transformations used to generate equivalent atoms: (a) $-x + 2, -y, -z + 1$; (b) $-x + 1, -y, -z + 1$; (c) $-x + 2, -y, -z + 2$. [b] Symmetry transformations used to generate equivalent atoms: (a) $-x + 1, -y, -z + 1$; (b) $x - 1, y, z$; (c) $-x + 1, -y, -z$; (d) $-x, -y, -z + 1$; (e) $-x, -y, -z$; (f) $x + 1, y, z$.

Results and Discussion

In earlier work, an examination of the dc magnetic susceptibility of the title compound, over the temperature range 2−300 K and in an applied field of 10 000 G, revealed a magnetic anomaly at around 135 K which suggested to us the possibility the compound was undergoing a structural phase transition at this temperature.[8] This prompted the currently reported extensive characterization of the material by employing a variety of techniques, work that revealed there were actually two phase transitions at around 151 and 135 K. Hence, we have identified three structural phases which we have labeled α, β, and γ (high-, medium-, and low-temperature phases, respectively). In section (a) below we describe the structures of the three phases as determined by single-crystal X-ray diffraction. The phase transitions themselves, as studied by (b) ac and dc susceptibilities and

(13) *teXsan: Crystal Structure Analysis Package*; Molecular Structure Corp.: The Woodlands, TX, 1985, 1992.
(14) Altomare, A.; Burla, M. C.; Cammalli, G.; Cascarano, M.; Giacovazzo, C.; Guagliardi, A.; Moliterni, A. G. G.; Polidori, G.; Spagna, A. *J. Appl. Crystallogr.* **1999**, *32*, 115.
(15) DIRDIF94: Beurskens, P. T.; Admiral, G.; Beurskens, G.; Bosman, W. P.; de Gelder, R.; Israel, R.; Smits, J. M. M. *The DIRDIF-94 program system*; Technical Report of the Crystallography Laboratory, University of Nijmegen: Nijmegen, The Netherlands, 1994.

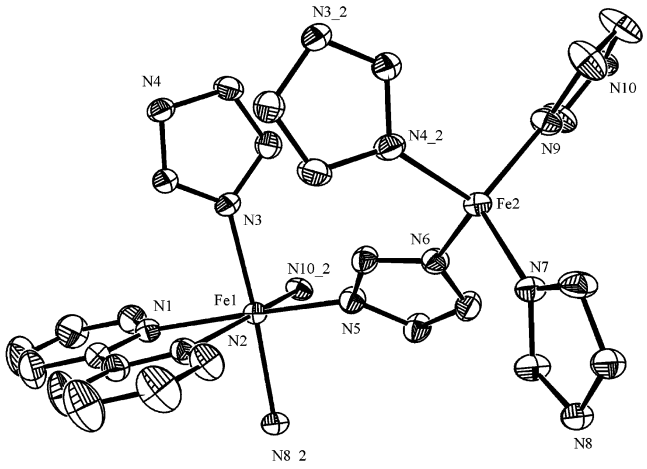

Figure 1. View of the asymmetric unit, expanded by inclusion of atoms (identified by the _2 symbolism) in symmetry-equivalent positions, of α-[Fe$_2$(imid)$_4$(bipy)]$_x$ showing the atom-numbering scheme. Probability thermal ellipsoids of 33% are shown.

(c) Mössbauer spectroscopy, are then discussed. The magnetic phase transition that occurs in the γ-phase material below 11 K was examined earlier by dc susceptibility studies.[8] In section d we describe further studies on this phenomenon employing both ac and dc magnetization techniques.

(a) Structures of α-, *β*-, and *γ*-Fe$_2$(imid)$_4$(bipy). Crystallographic data for α-Fe$_2$(imid)$_4$(bipy) are given in Table 1, and the asymmetric unit is shown in Figure 1. The 2D structure of this phase involves extended double-layer sheets. Sections of two of the sheets, viewed down the *c* axis, are depicted in Figure 2. In this figure the bipyridine ligands have been removed for clarity. The structure consists of alternating four- and six-coordinate high-spin iron(II) ions of approximate tetrahedral and octahedral geometry. Each iron is coordinated to four others by single bridging imidazolates, the six-coordinate ones being coordinated also by bipyridine ligands. The bipyridine ligands prevent bridging of metal centers in the third dimension and occupy space between the sheets, thereby isolating the sheets from each other. The iron ion connectivity diagram, which is similar to the one described below for the γ-phase, reveals connectivities between the two layers of a sheet forming four-membered rings and connectivities within the layers, top and bottom, forming six-membered fused rings.

Crystallographic data and the asymmetric unit for γ-Fe$_2$(imid)$_4$(bipy) are given in Table 1 and Figure 3. The volume of the unit cell in the γ-phase is approximately three times larger than the one in the α-phase, consistent with the 3-fold increase in the number of unique Fe(II) chromophores (Figures 1 and 3). The iron ion connectivity diagram for the γ-phase (Figure 4) is very similar to that of the α-phase,[8] and this similitude shows that the structural differences between the two phases are actually quite subtle. Nonetheless close examination of selected bond lengths and angles (Tables 2 and 3) for the phases reveals these differences.

Considering the FeN$_6$ chromophores (involving Fe(1) in the α-phase and Fe1a, Fe1b, and Fe1c in the γ-phase), for example, the Fe1b−N1b bond length is 2.217(2) Å in the γ-phase compared to the corresponding Fe(1)−N(1) distance of 2.262(2) Å in the α-phase while the respective distances for Fe1b−N2b and Fe(1)−N(2) are 2.313(2) and 2.299(2) Å. Similarly small differences in bond angles involving the FeN$_6$ chromophores can also be seen. For instance the N2b−Fe1b−N8b angle in the γ-phase corresponds to the N(2)−Fe(1)−N(8) angle in the α-phase, and while the first is 81.34(9)°, the second is 83.61(9)°. The adjacent N2b−Fe1b−N3b angle in the γ-phase at 91.08(8)° also differs from the corresponding α-phase N(2)−Fe(1)−N(3) angle of 89.68(9)°. The most distinctive FeN$_6$ bond parameters, however, involve the γ-phase Fe1c−N distances. These bond lengths range from 1.956(3) to 2.019(3) Å and average 1.996(3) Å. This compares with ranges of 2.152(3)−2.302(2) Å (average 2.208(3) Å) and 2.137(3)−2.313(2) Å (average 2.205(3) Å) for distances involving Fe1a and Fe1b, respectively, and with the range 2.153(2)−2.299(3) Å (average 2.209(3) Å) for the α-phase Fe1−N distances. That the average Fe−N distance involving Fe1c is some 0.2 Å shorter than those involving the other six coordinate iron(II) centers strongly suggests a low-spin configuration for Fe1c and high-spin configurations for the others.[16]

Small but significant differences can also be seen in bond lengths and angles involving the FeN$_4$ chromophores. For instance, Fe2b−N6b is 2.018(3) Å in the γ-phase compared to 2.036(2) Å for Fe(2)−N(6) in the α-phase and the N6b−Fe2b−N7b angle is 108.71(10)° in the γ-phase while the corresponding N(6)−Fe(2)−N(7) angle in the α-phase is 105.33(9)°.

While small changes to chromophore bond lengths and angles contribute to affecting the number of molecules in the asymmetric unit of Fe$_2$(imid)$_4$(bipy) and therefore the generation of different structural phases, so do molecular orientations within the unit cell. A careful comparison of the structures around the octahedral iron centers in the α- and γ-phases, for example, reveals differences in the two phases. This is illustrated in Figure 5, where the structures are overlapped around an octahedral center. In this construction, the metal atom, the bipy ligand, and one of the imidazolate ligands in each structure are overlapped. As can be seen, another imidazolate ligand (vertical position in the figure) orients differently in the two phases. Such rotational differences about the bridge axes appear to be a major structural difference between the phases of Fe$_2$(imid)$_4$(bipy).

Because of the relatively poor quality of the X-ray data for the β-phase, a detailed report on its structure is not possible at this time. Nonetheless our analysis does indicate a 6-fold increase in the number of unique Fe(II) chromophores in the β-phase over the α-phase, consistent with the approximate 6-fold increase in the unit cell volume (Table 1). The data analysis on the β-phase also supports an iron atom connectivity similar to those of the other two phases leading to the conclusion that the overall double-layer sheet structure is retained in this phase.

(b) Structural Phase Transitions Monitored by Dc and Ac Susceptibility Measurements. Our earlier dc magnetic

(16) Cotton, F. A.; Wilkinson, G.; Murillo, C. A.; Bochmann, M. *Advanced Inorganic Chemistry*, 6th ed.; Wiley: New York, 1999; p 785.

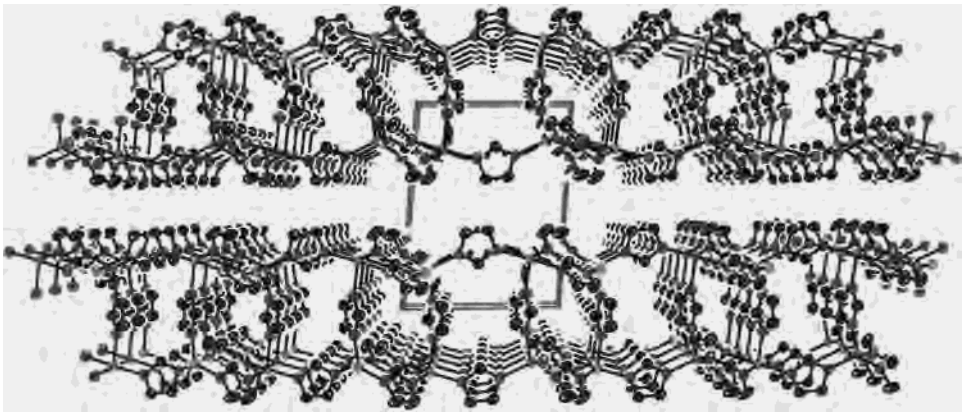

Figure 2. View of the crystal structure of α-$[Fe_2(imid)_4(bipy)]_x$ showing a section of two of the double-layer sheets. Bipyridine ligands have been removed for clarity; 50% thermal ellipsoids are shown.

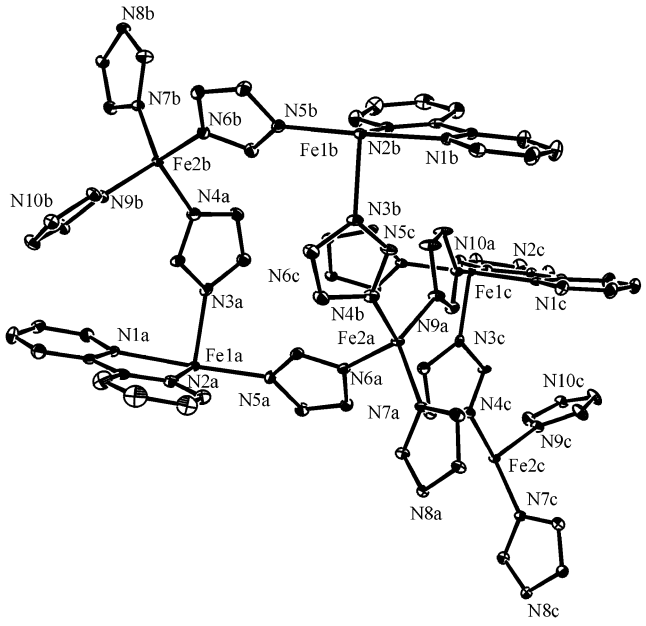

Figure 3. View of the asymmetric unit of γ-$[Fe_2(imid)_4(bipy)]_x$ showing the atom-numbering scheme. Probability thermal ellipsoids of 33% are shown.

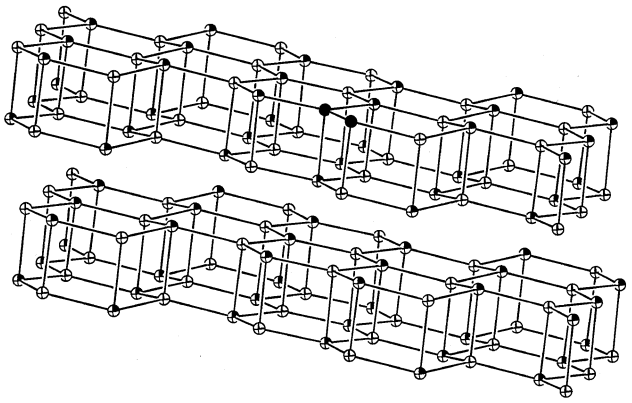

Figure 4. Iron ion connectivity diagram of a section of two double-layer sheets of γ-$[Fe_2(imid)_4(bipy)]_x$: octahedral Fe, shaded ellipsoids; tetrahedral Fe, open ellipsoids (33% standard spheres).

susceptibility studies at applied fields of 500 G and 10 000 G, over the temperature range 2−300 K, clearly revealed the low-temperature magnetic phase transition and a magnetic anomaly now identified as the $\beta \rightarrow \gamma$ phase transition. Closer

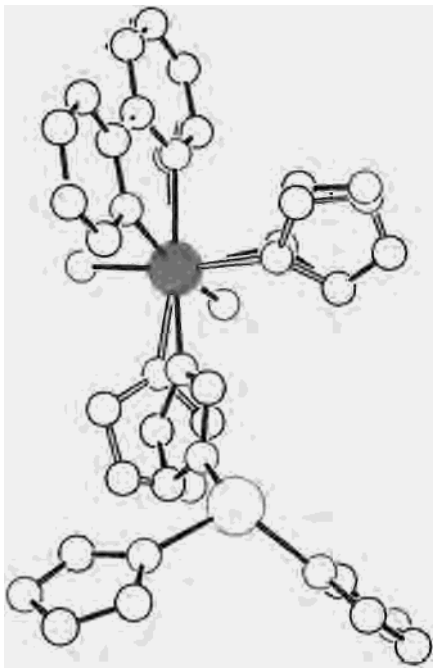

Figure 5. Comparison of octahedral coordination sphere geometries in α- and γ-phases of $[Fe_2(imid)_4(bipy)]_x$.

examination of this earlier data over the entire temperature range studied reveals a second, weaker, anomaly at higher temperatures now recognized as the $\alpha \rightarrow \beta$ transition. In an effort to better characterize the structural phase transitions and to determine transition temperatures accurately, we performed dc susceptibility measurements at an applied field of 1000 G in both cooling and heating modes. Also, for higher accuracy, a higher density data acquisition was utilized close to the phase transitions. In Figure 6, the temperature dependence of χT (100−190 K) is shown. In the cooling mode, χT decreases slightly until it reaches ∼152 K and then it decreases abruptly until ∼150 K ($\alpha \rightarrow \beta$) attaining a "plateau" between ∼150 and 138 K. Finally, χT diminishes abruptly over the range ∼138−132 K ($\beta \rightarrow \gamma$) before "leveling" again. In the warming mode, the temperature range at which the $\gamma \rightarrow \beta$ transition occurs is about 5 deg higher than that at which the $\beta \rightarrow \gamma$ transition occurred, giving rise to a noticeable hysteresis (Figure 6). Above 137 K, and following a warming mode, χT increases gradually, following

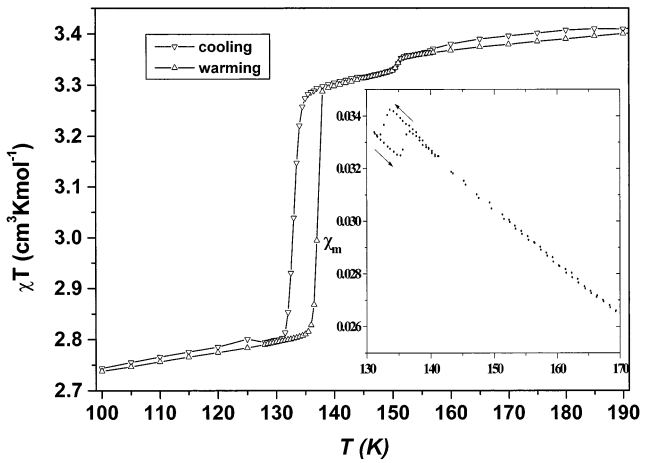

Figure 6. χT versus T plot plots in cooling and warming modes. H_{dc} = 1 000 G. The insert shows χ versus T plots in cooling and warming modes. H_{ac} = 2.5 G, and f = 500 Hz.

the cooling curve in this region quite closely. The value of χT then increases abruptly over the ~150−152 K region ($\beta \rightarrow \alpha$), again following the cooling mode closely. In contrast to the $\beta \leftrightarrow \gamma$ transition, there appears to be no significant hysteresis associated with the $\beta \leftrightarrow \alpha$ transition. To more accurately define the transition temperatures, the temperature dependence of the derivative d(χT)/χT, in cooling and warming modes, was examined. This gave transition temperatures of 151 K for the $\alpha \leftrightarrow \beta$ transition and 135 K for the $\beta \leftrightarrow \gamma$ transition, the latter with a thermal hysteresis width of 4 K (133−137 K).

Employing high-resolution ac susceptibility measurements, in both cooling and warming modes, we were able to observe the low-temperature $\beta \leftrightarrow \gamma$ transition (Figure 6) but not the more weakly magnetically observable $\alpha \leftrightarrow \beta$ transition. These studies confirmed the hysteretic properties of the $\beta \leftrightarrow \gamma$ transition, and a plot of d(χT)/χT employing the ac data confirmed the temperature as 135 K with a thermal hysteresis width of 4 K.

The $\alpha \rightarrow \beta$ and $\beta \rightarrow \gamma$ transitions are marked by abrupt decreases in χT (Figure 6). A possible explanation for this behavior is that accompanying the structural phase transitions are changes in spin state of some of the metal centers. To test this theory, a detailed analysis of the 1000 G dc magnetic susceptibility (warming mode) data over the temperature range 250−100 K was made. The data in both the 250−155 K range (α-phase) and the 134−100 K range (γ-phase) obey the Curie−Weiss law. The data in the high-temperature, α-phase region were fit to the Curie−Weiss expression $\chi = C/(T + \Theta)$, employing C and Θ as variable parameters. An excellent fit was obtained with the best-fit parameters, C = 3.564 and Θ = 9.35. The data over the lower temperature γ-phase region were then analyzed by assuming a fraction, $1 - f$, of the iron centers are low-spin $S = 0$ and the rest are $S = 2$ centers that obey the same Curie−Weiss Law as determined for the α-phase. The data in the 134−100 K range were fit to the modified Curie−Weiss expression $\chi = f[3.564/(T + 9.35)]$, where f, the fraction of magnetically active centers, was employed as a variable. An excellent best fit was obtained for f = 0.840. This result is consistent with

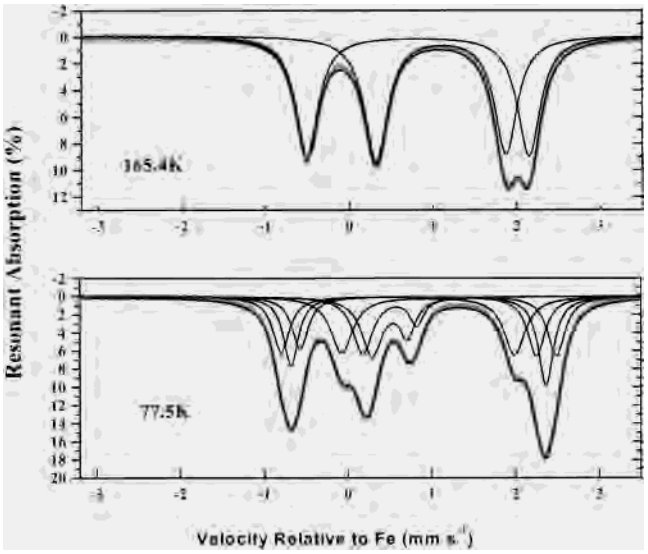

Figure 7. Mössbauer spectra at 165.4 and 77.5 K.

Table 4. Mössbauer Spectroscopy Parameters

T, K	site	δ,[a] mm/s	ΔE, mm/s	intensity, %
293	"O_h" (2,3)[b]	1.01	1.06	52.2
	"T_d" (1,4)	0.74	2.75	47.8
165.4	"O_h" (2,3)	1.10	1.55	50.5
	"T_d" (1,4)	0.82	2.65	49.5
77.5	"O_h" (4,9)	0.96	2.06	20.6
	"O_h" (5,8)	0.51	0.65	12.7
	"O_h" (6,7)	0.50	0.42	14.9
	"T_d" (1,12)	0.85	3.29	15.5
	"T_d" (2,11)	0.85	3.05	19.2
	"T_d" (3,10)	0.84	2.83	17.1

[a] Relative to natural Fe foil at 293 K. [b] The integers refer to the transitions of Figure 7 reading left to right while intensity (%) refers to the designated quadrupole doublets. Line widths Γ_i ranged between the extremes 0.25−0.31 mm/s.

the picture that while all iron centers in the α-phase are high-spin $S = 2$, in the γ-phase 16% are low-spin $S = 0$. The abrupt decreases in χT observed at the $\alpha \rightarrow \beta$ and $\beta \rightarrow \gamma$ transitions may then be explained by $S = 2$ to $S = 0$ spin-state transitions of, overall, 1 in 6 of the iron centers. The conclusion reached earlier in the analysis of crystallographic data that Fe1c in the γ-phase (1 in 6 of the iron centers) is low-spin is consistent with this magnetic analysis. Further support for the existence of $S = 0$ iron centers in the γ-phase was also obtained from low-temperature Mössbauer spectra, and this evidence will be presented in section c, which follows.

(c) Structural Phase Transitions Monitored by Mössbauer Spectroscopy. The room-temperature Mössbauer spectrum of the title compound is essentially identical with that observed at 165.4 K, top of Figure 7. The latter corresponds to two overlapping quadrupole doublets, indicated in the figure, whose parameters (Table 4) are typical of pseudotetrahedral (outer doublet, peaks 1,4) and pseudooctahedral high-spin iron(II) (inner doublet, peaks 2,3) and with intensity ratio ~1 consistent with the structure determined for the α-phase.[8] The foregoing transition associations as opposed to (1,3-"T_d") and (2,4-"O_h") for the quadrupole doublets are most consistent with isomer shifts established

for such sites for similar ligation[8,17,18] and the expected increase (~0.08 to 0.1 mm/s) in δ owing to the second-order Doppler shift on cooling from ambient T to ~165 K. At 77.5 K, the spectrum changes to the complex one at the bottom of Figure 7, an unconstrained fit corresponding to six independent quadrupole doublets whose parameters and relative intensities are likewise given in Table 4. This observation is again consistent with X-ray results for the γ-phase, i.e., the requirement of six highly overlapped quadrupole doublets. These correspond to three slightly different (nominally) T_d doublets (reading left to right: peak pairs 1,12, 2,11, and 3,10) and three O_h environment doublets (peak pairs 4,9, 5,8, and 6,7). The isomer shifts (δ) of the "T_d" doublets are typical of tetrahedral high-spin iron(II) for the ligation involved.[17] The isomer shift of the octahedral iron(II) doublet (4,9) is also fully consistent with spin-quintet ground-state iron(II) for the ligation at these sites.[18] On the other hand, the δ values for doublets 5,8 and 6,7 are significantly less than the latter and suggest a spin-state change to either $S = 0$[19−21] or even $S = 1$ iron(II).[19] However, distinguishing these ground spin state possibilities on the basis of isomer shifts alone is difficult and unreliable at best.[22] We will come back to this problem in the consideration of smaller velocity sweep Mössbauer spectra between ~10 and 1.2 K (vide infra), which appear to suggest a singlet ground state, the more common observation[19] in this context. The Mössbauer results suggest that ~28% of the iron(II) sites in the material have $S = 0$. In light of the present discussion, it is appropriate to refer the reader to the earlier discussion where structural and magnetic evidence was provided for spin-crossover behavior for a fraction (at least one-sixth, or ~17%) of the "O_h" sites. The apparent discrepancy between the Mössbauer results on one hand and the magnetic susceptibility and X-ray results on the other could arise because of different recoil free fractions for the six sites or a partial spin transition at an iron site. We mention that there is recent precedence[21] for a crystallographic phase transition (albeit in a mononuclear six coordinate high-spin iron(II) compound) in which only a fraction of the "O_h" iron(II) present at ambient temperature undergoes a spin state change.

Mössbauer spectra were collected at various temperatures in both warming and cooling modes. These experiments confirmed both of the structural phase transitions. In fact it is interesting to note that the high-temperature $\alpha \leftrightarrow \beta$ transition, which is relatively difficult to monitor by magnetic studies, is seen clearly in the Mössbauer studies and was in fact first observed by this technique. We hasten to point out

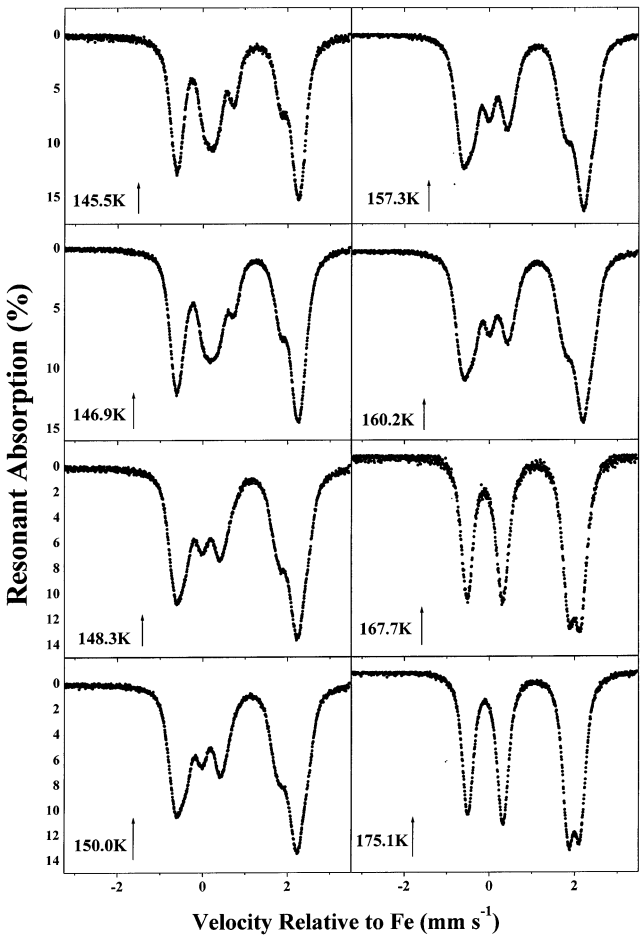

Figure 8. Mössbauer spectra in the warming mode.

that the spectra were obtained for material "gently mulled with Apiezon-N grease" to immobilize and protect the sample and ensure good thermal contact. Care was taken not to pulverize the sample by grinding. Previous experience[23] indicates that while this procedure can be helpful to achieving an isotropic absorber free of texture/orientation effects (a desirable goal in certain circumstances); it can also introduce defects that hinder or completely prevent crystallographic phase transitions, especially for layered systems. Spectra obtained in the warming mode, shown in Figure 8, indicate the $\gamma \rightarrow \beta$ transition occurs between 147 and 148 K while the $\beta \rightarrow \gamma$ transition is between 160 and 168 K. These same transitions are seen between 140 and 145 K and between 163 and 165 K, respectively, when spectra are obtained in the cooling mode (Figure 9). Consistent with the data obtained from susceptibility studies the Mössbauer spectra show evidence of thermal hysteresis of around 3−5 K in the $\beta \leftrightarrow \gamma$ transition. To date, hysteresis for the $\alpha \leftrightarrow \beta$ transition has not been investigated in detail using Mössbauer spectroscopy. However, both transitions appear to occur at ~10 K higher in the Mössbauer studies than for the dc and ac determinations. This is not the result of thermometry differences between the different experiments (see the Experimental Section). In careful studies of spin crossovers of high-spin iron(II) complexes (generally hysteretic first-

(17) Long, G. J.; Grandjean, F.; Trofimenko, S. *Inorg. Chem.* **1993**, *32*, 1055.
(18) Reger, D. L.; Little, C. A.; Rheingold, A. L.; Sommer, R.; Long, G. L. *Inorg Chim. Acta* **2001**, *316*, 67.
(19) Gutlich, P.; Hauser, A.; Spiering, H. *Angew. Chem., Int. Ed. Engl.* **1994**, *33*, 2024.
(20) van Koningsbruggen, P. J.; Garcia, J.; Kahn, O.; Fournès, L.; Koojman, H.; Spek, A. J.; Haasnoot, J. G.; Moscovici, J.; Provost, K.; Michalowicz, A.; Renz, F.; Gutlich, P. *Inorg. Chem.* **2000**, *39*, 1891.
(21) Reger, D. L.; Little, C. A.; Rheingold, A. L.; Lam, M., Liable-Sands, L. M.; Rhagitan, B.; Concolino, T.; Mohan, A.; Long, G. J.; Briois, V.; Grandjean, F. *Inorg. Chem.* **2001**, *40*, 1508.
(22) Reiff, W. M.; Wong, H.; Baldwin, J. E.; Huff, J. *Inorg. Chim. Acta* **1977**, *25*, 91.
(23) Nicolini, C.; Reiff, W. M. *Inorg. Chim. Acta* **1983**, *68*, 55.

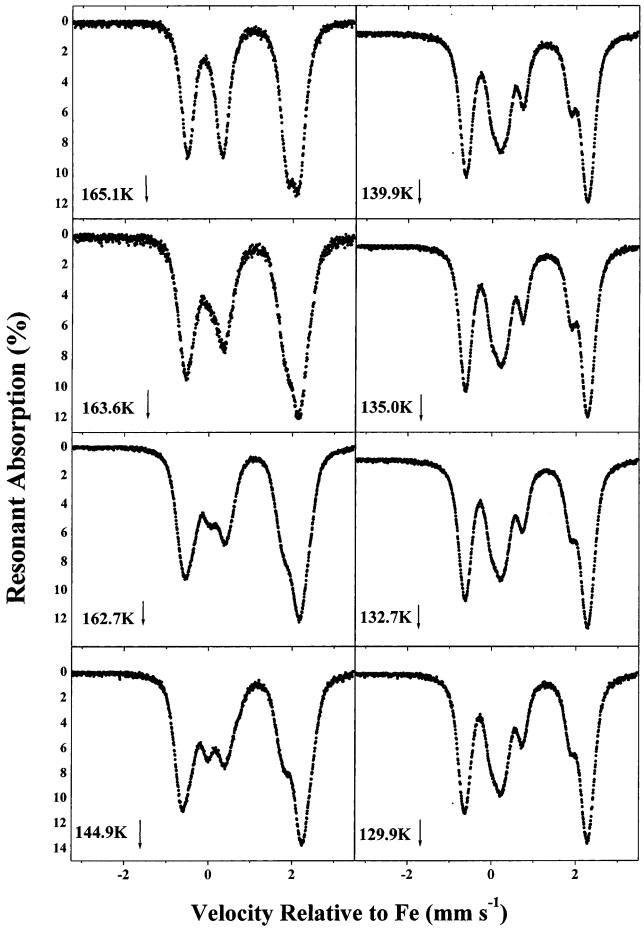

Figure 9. Mössbauer spectra in the cooling mode.

order transitions) and with careful cross-calibration of the thermometry involved, "bulk" techniques such as the temperature dependence of magnetic susceptibility or heat capacity have been compared to spectroscopic methods such as the Mössbauer effect. The latter is found to manifest the crossover behavior "earlier", i.e., at higher temperature in cooling mode. This is attributable to the existence of a definite time window for the spectroscopic method while bulk magnetic measurements at thermodynamic equilibrium correspond to no time window per se.[24] We summarize this section by stating that considering the limitations of the primary techniques applied (bulk susceptibility and Mossbauer spectroscopy measurements) and the complexity of the β and γ phases, a minimum of one-sixth of the "O_h" iron sites of ambient temperature undergo spin crossovers to what are likely spin singlet ground states.

(d) Low-Temperature Magnetic Phase Transition. Earlier dc magnetic susceptibility studies revealed an abrupt increase in the magnetic moment of $Fe_2(imid)_4(bipy)$ below ~11 K, ascribed to a transition to a net, nonzero moment, 3D ordered ground state.[8] A study at 4.8 K revealed magnetic hysteresis with a remnant magnetization of 200 cm^3 G mol^{-1} and a coercive field of 15 G.[8] In an effort to determine more accurately the onset of the magnetic transition in γ-$Fe_2(imid)_4(bipy)$, the temperature dependences of the field-cooled magnetization (FCM), zero-field-cooled magnetization (ZFCM), and remnant magnetization (REM) were examined as were the ac susceptibilities (Figure 10 and insert). The FCM curve, measured on cooling the sample in a dc field of 50 G, and the ZFCM curve, measured by cooling the sample in zero field and then warming in a 50 G dc field, show the onset of an increase in magnetization in the 6−8 K region and a maximum in the 2−3 K region. The derivative curves, d(FCM)/dT and d(ZFCM)/dT, minimize in the 3.5−4 K region, the region below which the FCM and ZFCM curves diverge. These studies give the critical temperature T_c as 4 K.[3] The temperature at which REM (obtained by cooling the sample in a 50 G dc field and then collecting data while warming in zero field) vanishes is difficult to obtain accurately; nonetheless, inspection of Figure 10 shows this to occur, as expected, in the region of T_c.

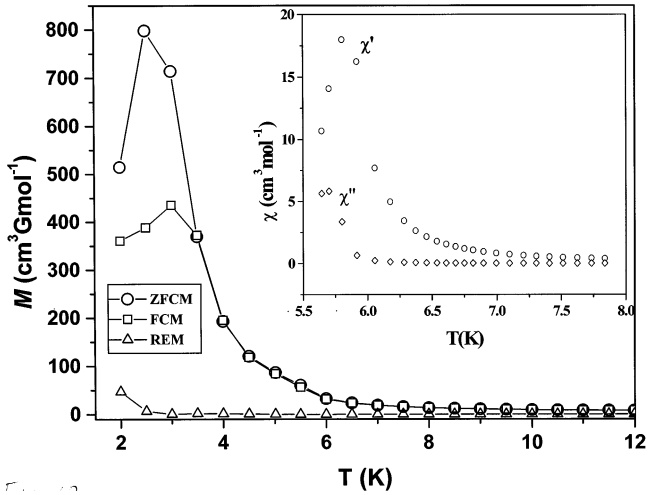

Figure 10. Plots of ZFCM, FCM, and REM versus temperature. H_{dc} = 50 G. The insert shows temperature dependence of in-phase, χ', and out-of phase, χ'', susceptibilities. H_{ac} = 1 G, and f = 125 Hz.

The ac susceptibility data, obtained in a zero static (dc) field and a 125 Hz oscillating field of 1 G, are shown in the Figure 10 insert. The in-phase, χ', and out-of-phase, χ'', susceptibilities diverge below ~8 K and maximize in the 5.5−6 K region in reasonable agreement with T_c indicated by Mössbauer spectra (vide infra). In particular, the observation of nonzero χ'' below 6 K further verifies the onset of a nonzero moment below this temperature.

A perhaps more direct method for determining the critical temperature (at least for iron compounds) is a microscopic spectroscopic technique such as Mössbauer spectroscopy as opposed to bulk ac and dc susceptibility measurements. In this context, sample spectra showing the (low) temperature dependence of the Mössbauer spectrum of the title compound are presented in Figures 11−13. The critical temperature corresponding to the transition from the rapidly relaxing paramagnetic phase to long-range order is 6.5 ± 0.5 K as indicated from the Mössbauer spectra in Figure 11. The X-ray structure and Mössbauer spectrum at 77 K indicate six iron environments for the γ-phase. A comparison of the spectrum at the bottom of Figure 7 with that at the top of Figure 13 reveals that the structure of the γ-phase persists down to

(24) Gutlich, P. Private communication.

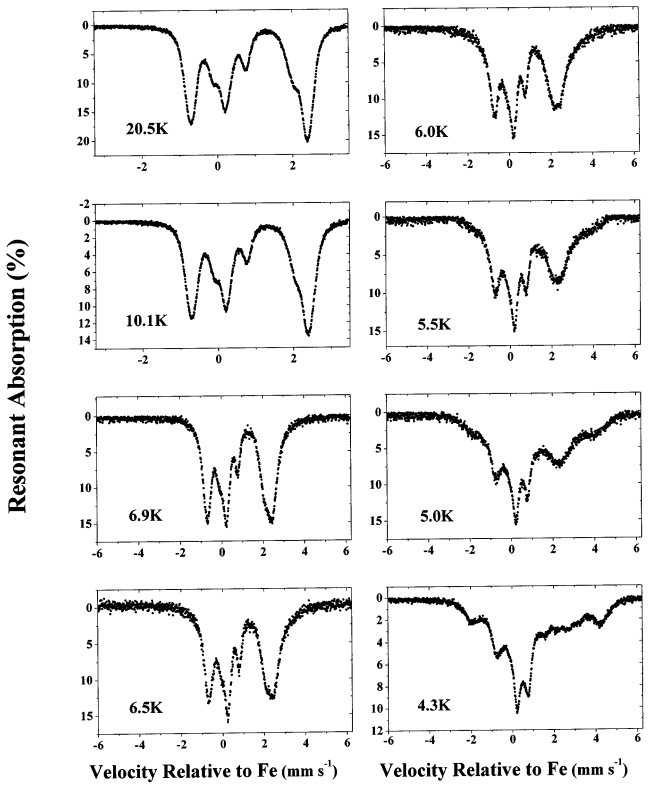

Figure 11. Temperature dependence of Mössbauer spectra for the γ-phase for $T \leq 20.5$ K.

8.5 K. Thus, assuming that the γ-phase molecular structure prevails at $T \leq \sim 6.5$ K, one can potentially observe from 36 to 48 γ-ray transitions for the hyperfine spectrum of the ordered state at full resolution. The latter situation corresponds to nonzero intensity for the normally forbidden $\Delta m_I = \pm 2$ transitions, a distinct possibility for high-spin iron(II). In any event, it is clear from the spectrum at 4.2 K that we do not have anything near full resolution. This is not surprising for a system composed of three slightly different pseudotetrahedral and -octahedral coordination environments. In this light, we have made no attempt to deconvolute the low-temperature spectra. Suffice it to say that the maximum nuclear Zeeman splitting of Figure 11 spans ~6.25 mm/s corresponding to an internal field (H_n) of ~19.5 T. This value is fairly typical of high-spin iron(II) environments for which the expected Fermi contact term, ~40 T, is significantly reduced by a substantial opposing orbital contribution to H_n and to a lesser extent by covalency effects.[25] Although the spectrum sharpens somewhat with approach to magnetic saturation at 1.2 K (Figure 12), the resolution in the context of reliable fitting for multiple, overlapping, hyperfine patterns is not measurably enhanced.

Finally, in Figure 13, we show a series of spectra above and below T_c at smaller (expanded) velocity sweeps (half the velocity sweep of Figures 11 and 12). The intensity previously attributed to a low-spin iron(II) fraction resulting from a spin crossover is denoted by a stick diagram in the center of the spectrum at 8.5 K. This spectrum is essentially

(25) Greenwood, N. N.; Gibb, T. C. *Mössbauer Spectroscopy*; Chapman & Hall: London, 1971.

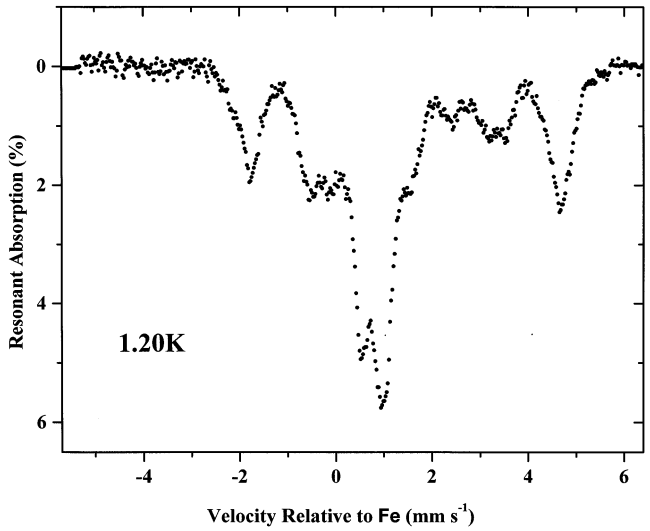

Figure 12. Mössbauer spectrum of the γ-phase at 1.2 K.

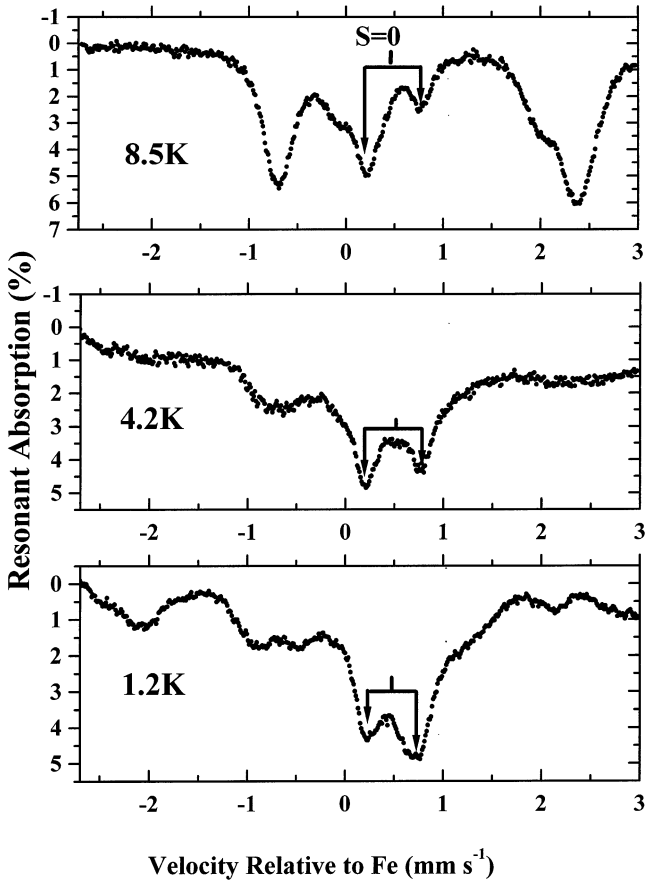

Figure 13. Expanded velocity sweep Mössbauer spectra of the γ-phase above and below T_c.

identical with that deconvoluted at 77.5 K (bottom of Figure 7) save that the latter corresponds to 1024 data channels while those of Figure 13 are the standard 512 channels. In any event, it appears that the central intensity persists, unshifted, well below T_c. This is precisely the behavior expected for diamagnetic, spin singlet ($S = 0$) ground iron(II) and accords with the more common observation[19] of an $S = 2 \rightarrow S = 0$ spin crossover as opposed to $S = 2 \rightarrow S = 1$. Herein, we are assuming that (1) if the ground state were

a spin triplet for ferrous ions that participate in the magnetic ordering and (2) provided that this $S = 1$ iron is not strongly zero-field split (D large and positive) leading to nonmagnetic $M_S = 0$ ground levels, then such triplets are likely to undergo magnetic hyperfine splitting as a direct result of ordering leading to a decrease in their intensity in the velocity region under consideration.

Summary and Conclusions

$Fe_2(imid)_4(bipy)$ is unusual in presenting two structural phase transitions, spin-state transition(s), and a transition to a magnetically ordered state over the temperature range from ambient to 2 K. Detailed ac and dc magnetization measurements revealed thermal hysteresis of about 4 K in the low-temperature structural phase transition and no obvious hysteresis in the high-temperature transition. Single-crystal X-ray diffraction studies on the three structural phases reveal that the basic metal−ligand connectivities as well as general chromophore geometries of the three are the same. All three have structures involving extended 2D double-layer sheets of alternating tetrahedral and octahedral iron ion centers, each iron bridged to four others by single imidazolate ligands. Chelating bipyridine ligands occupy the extra coordination sites on the octahedral centers. Relatively minor differences in chromophore geometries affect the number of unique iron centers thereby distinguishing the three structural phases. This relatively modest difference in the structures clearly explains the facile conversion of one phase to another in a process in which the crystal integrity is maintained. On the other hand, it is interesting to note that the effect of these relatively modest structural differences is readily detectable by Mössbauer spectroscopy and both ac and dc magnetization studies. Structural, magnetic, and Mössbauer studies combined reveal that the overall structural changes on going from α to β to γ are accompanied by spin-crossover behavior in which at least 1 in 6 of the iron(II) sites change from high-spin $S = 2$ to low-spin $S = 0$ configurations. In passing, we note that the related $Fe_2(imid)_4$(5,5′-dimethyl-2,2′bipyridine) has a layered structure similar to the title compound but is somewhat less complicated in that it exhibits a single crystallographic phase transition. This transition is accompanied by a more readily observed spin crossover vis-à-vis the present study.[26]

The new studies presented here on the magnetic phase transition have not provided a definitive understanding of the mechanism by which it occurs. As suggested previously,[8] this probably involves a combination of spin canting and ferrimagnetism generating uncompensated moments on the 2D lattice which, below a critical temperature, align ferromagnetically thus generating the observed behavior. The current studies, performed at much lower applied fields that the earlier ones, have confirmed the magnetic ordering and have permitted a better evaluation of the temperature at which it occurs. The earlier higher field measurements showed only that the transition occurs below 11 K. On the basis of the measurements reported here, T_c is significantly lower, i.e. ~6.5 K.

Acknowledgment. A.S. and R.C.T. thank the Natural Sciences and Engineering Research Council of Canada for financial support and P. Borda of this department for C, H, and N analyses. W.M.R. is pleased to acknowledge the U.S. NSF for funding toward the purchase of an ac susceptometer and dc/ac SQUID magnetometer.

Supporting Information Available: Complete details of the crystallographic study of the α- and γ-forms of poly[(2,2′-bipyridine)tetrakis(imidazolato)diiron(II)] (CIF). This material is available free of charge via the Internet at http://pubs.acs.org.

IC030170N

(26) Patrick, B. O.; Reiff, W. M.; Sanchez, V.; Storr, A.; Thompson, R. C. To be published.